PERGAMON

Journal of Structural Geology 25 (2003) 1855–1873

JOURNAL OF STRUCTURAL GEOLOGY

www.elsevier.com/locate/jsg

Microfracture analysis of fault growth and wear processes, Punchbowl Fault, San Andreas system, California

J.E. Wilson[1], J.S. Chester*, F.M. Chester

Center for Tectonophysics, Department of Geology & Geophysics, Texas A&M University, College Station, TX 77843, USA

Received 27 January 2002; accepted 7 February 2003

Abstract

Fabric and timing relations of mode I microfractures are used to test current hypotheses for the origin of damage along large-displacement faults by the processes of fault growth and wear. Oriented samples 0.075 m to 1 km from the Punchbowl fault surface (i.e. ultracataclasite layer) document an increase in development of preferred orientation and increase in density of microfractures towards the ultracataclasite layer, defining a zone of fault-related microfracture damage about 100 m thick. A distinct microfracture set that is perpendicular to the slip direction of the fault is present throughout the damage zone. This implies that the average orientation of the maximum principal compressive stress within the damage zone was nearly normal to the fault surface. Two additional microfracture sets are present, one oriented at low angles to the fault within meters of the ultracataclasite layer, and another low-angle set that occurs in the outermost damage zone. The preferred orientations and timing relations are most consistent with local damage accumulation from stress cycling associated with slip on a geometrically irregular, relatively weak fault surface. Low-angle microfractures nearest the ultracataclasite layer also may record wear associated with the passage of earthquake ruptures, and those in the outermost damage zone may be consistent with Andersonian fault formation and subsequent fault weakening.

Keywords: Faulting; Microfracture; Fault growth; Damage zone; Earthquakes; Fault mechanics

1. Introduction

Large-displacement, brittle fault zones often are characterized by one or more relatively narrow zones (several meters thick) of intense deformation, referred to as the fault-core, surrounded by a broader zone (hundreds of meters thick) of deformed rock, referred to as the damage zone, that grades outward into undeformed host-rock (e.g. Flinn, 1977; Wallace and Morris, 1986; Chester et al., 1993). Several studies have identified an inward intensification of fractures, subsidiary faults, cataclastic particle size reduction, and mineral alteration toward the fault-core (e.g. Chester and Logan, 1986; Anders and Wiltschko, 1994; Evans and Chester, 1995; Schulz and Evans, 1998), as well as a preferred orientation of subsidiary faults and joints (Friedman, 1969; Brock and Engelder, 1977; Chester and Logan, 1987; Chester et al., 1993; Anders and Wiltschko, 1994; Bruhn et al., 1994; Little, 1995). The purpose of this paper is to determine the orientation and distribution of microfractures, and timing of microfracture development, along the large-displacement Punchbowl fault to test current hypotheses for the origin of damage along faults by the processes of fault growth and wear.

Opening mode microfractures form in an orientation perpendicular to the local minimum compressive principal stress direction (Friedman, 1963; Engelder, 1974). Provided that statistically based sampling and analysis techniques are employed, microfracture fabrics may be used to define the paleostress conditions in the rock at the time the microfractures formed (e.g. Friedman, 1963, 1969; Lespinasse and Pecher, 1986; Kowallis et al., 1987; Laubach, 1989, 1997; Blenkinsop, 1990; Blenkinsop and Sibson, 1992). The fabric of microfractures clearly related to faulting, such as those in the damage zone of a fault, may record the spatial and temporal variations in fault stress state, and thus may be used to test the predictions of fault mechanical models (e.g. Vermilye and Scholz, 1998).

* Corresponding author. Tel.: +1-979-845-1380; fax: +1-979-845-6162.
E-mail address: chesterj@geo.tamu.edu (J.S. Chester).
[1] Now at: Earth and Environmental Science Department, New Mexico Tech, Socorro, New Mexico 87801.

0191-8141/03/$ - see front matter © 2003 Elsevier Ltd. All rights reserved.
doi:10.1016/S0191-8141(03)00036-1

Microfractures and other damage elements are expected to form during early stages of fault formation and growth. As described by Anderson's theory of faulting (Anderson, 1942), faults form at acute angles (~25–30°) with the maximum principal compressive stress direction for brittle deformation of the upper crust. Assuming that stress states are relatively homogeneous and that microfractures form during faulting, one might expect microfracture fabrics to display preferred orientations consistent with Andersonian faulting (Fig. 1A). However, stress inhomogeneity and concentration are expected along faults, and these variations also may influence the microfracture fabric of damage zones, particularly near the fault surface. Microfractures formed during fault growth may reflect stress concentrations at propagating fault tips and in linkage zones (e.g. Cowie and Scholz, 1992; Vermilye and Scholz, 1998). Damage also may develop along faults during later stages of deformation in response to stress cycling associated with displacement along and juxtaposition of geometrically irregular fault surfaces (e.g. Flinn, 1977; Sibson, 1986) and earthquake rupturing (e.g. Sibson, 1989).

Models of fault growth, based on linear elastic fracture mechanics and cohesive crack models consider the inelastic deformation about a fault tip as it propagates through intact rock (e.g. Cowie and Scholz, 1992). The inelastic zone of deformation, also called the process zone (e.g. Scholz et al., 1993), is represented, in part, by zones of intense microfracturing. As a fault grows, the fault tip and associated process zone propagate, leaving a zone of damaged rock in its wake. Thus, the fault growth model predicts that the microfracture fabric of the damaged zone surrounding the fault surface forms early in the fault history and reflects fault-tip stress orientations (Fig. 1B).

Wear models focus on the progressive accumulation of damage resulting from displacement on an established surface (Sibson, 1986; Scholz, 1987). Fault surfaces are rough at all scales (e.g. Scholz and Aviles, 1986; Power and Tullis, 1991). Displacement along a rough surface produces geometric mismatch and local stress concentration. With continued slip, the rock adjacent to a fault surface experiences stress cycling in response to the passing of geometric irregularities. This cycling leads to continued fracturing and wear. The zone of damage is expected to increase in overall thickness with displacement because increasingly larger irregularities are juxtaposed with increased displacements (e.g. Scholz, 1987). Analysis of stress states induced by slip along a non-planar frictionless fault suggests that the maximum compressive stress varies locally from a fault-normal to a fault-parallel orientation (e.g. Saucier et al., 1992; Chester and Fletcher, 1997). On the basis of mechanical analysis of slip along non-planar faults with friction (Chester and Chester, 2000), fractures most likely occur at angles to the fault that are slightly greater than the far-field maximum compressive stress (Fig. 1C). Thus, the wear model predicts that microfractures in the zone of damage surrounding a fault should record the

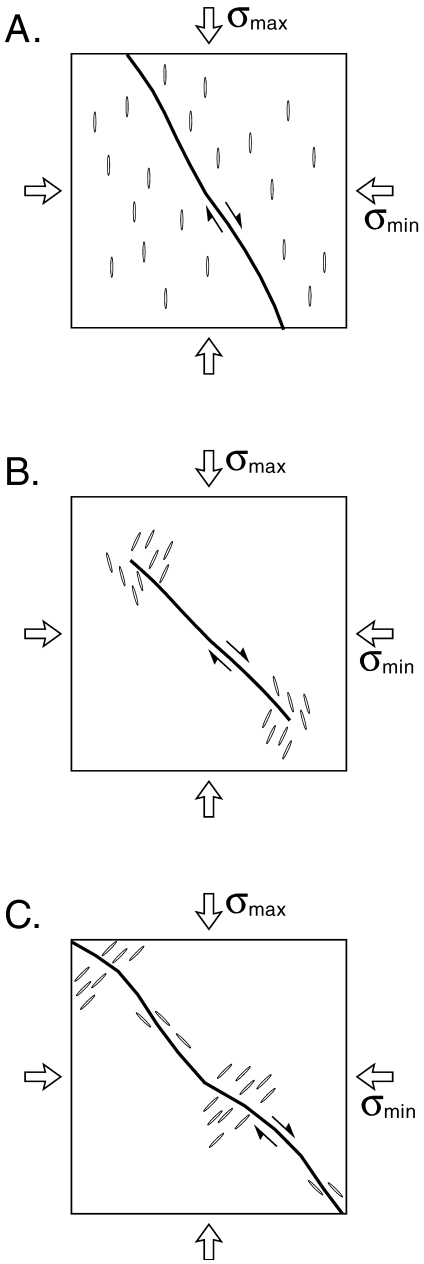

Fig. 1. Schematic diagrams illustrating mechanics-based models for microfracture development associated with fault formation and wear. (A) Fault models assuming homogeneous stress. Anderson model for fault formation predicts microfracture orientation at approximately 30° to fault. Wear models predict microfractures form at 50–70° to fault for frictional sliding at limiting condition or for weak faults. (B) Fault model for fault growth by tip propagation. Microfractures form in the region of the fault-tip stress concentration. Depending on mode of tip propagation, microfractures are expected to form at orientations different than far-field principal stress directions. (C) Fault model for wear along wavy, frictional fault surfaces. Microfractures expected to form in the region of stress concentrations formed by offset along rough surfaces. Microfractures generally predicted to form at orientations different than far-field. For some loading conditions and weak faults, microfractures form approximately normal and parallel to the fault surface.

entire history of faulting, with the most extensive deformation associated with the final stages of fault movement.

Several studies have investigated the structural development and accumulation of damage along small faults having displacements up to tens of meters (e.g. Martel, 1990; Vermilye and Scholz, 1998; Shipton and Cowie, 2001). A complementary approach, employed in this work, is to investigate the fracture fabric in the damage zone of a large-displacement fault (i.e. displacement on the order of tens of kilometers), and to use temporal relations to determine the processes of damage accumulation. The Punchbowl fault zone was chosen for this study because the macroscopic and mesoscopic character of the fault is well established (e.g. Chester and Logan, 1986, 1987; Chester and Chester, 1998; Chester et al., 2003). Previously collected structural data provide independent information on the state of stress and distribution of damage about the fault, and provide a basis to analyze the microfracture data.

2. Geology of the Punchbowl fault

The Punchbowl fault is an inactive, exhumed fault of the San Andreas transform system located near the boundary between the San Gabriel Mountains and Mojave Desert, central Transverse Ranges, southern California (Fig. 2). It is located approximately 5 km southwest of and is parallel to the active strand of the San Andreas fault. The Punchbowl fault is truncated to the northwest and to the southeast by the San Andreas and is considered an abandoned strand of the San Andreas system (Dibblee, 1968, 1987; Weldon et al., 1993). The fault commonly displays sinuous and paired traces that cut crystalline rock of the San Gabriel basement complex and folded Paleocene and younger sedimentary rocks (Noble, 1954). Correlation of stratigraphic units and structural features across the San Andreas and Punchbowl faults in the Sierra Pelona Mountains, San Gabriel Mountains, and Orocopia Mountains indicates that the Punchbowl fault accounts for 44 km of right-lateral separation in the Late-Miocene and Pliocene (Dibblee, 1968; Weldon et al., 1993).

The portion of the fault studied is located in Devil's Punchbowl Los Angeles County Park, where the Punchbowl fault consists of two main fault strands that bound a slice of fractured and faulted San Gabriel basement complex up to 0.5 km in thickness (Fig. 3). The slice of fractured basement between the northern and southern fault strands contains a heterogeneous assemblage of Precambrian biotite gneiss and quartzofeldspathic gneiss with alternating leucocratic and melanocratic bands, and massive to foliated Cretaceous plutonic rocks including quartz diorite, tonalite, granodiorite, and biotite monzogranite (Cox et al., 1983). The southernmost fault strand is not always well developed, is segmented and discontinuous, and probably accounts for only a few kilometers of right-lateral separation (Chester, unpublished mapping, 1995). The northernmost fault strand is well developed. The northern strand is a reverse-oblique, strike-slip fault that dips steeply to the southwest, placing cataclastically deformed crystalline basement over folded Punchbowl Formation along a single, continuous ultracataclasite layer that is approximately 0.3 m thick (Chester and Logan, 1986). Previous structural studies indicate that at least 10 km, but most likely upwards of 40 km of right-lateral displacement was accommodated on the northernmost trace of the Punchbowl fault zone (Chester and Chester, 1998).

The Punchbowl Formation, on the north side of the fault, likely was deposited in a pull-apart basin during the early

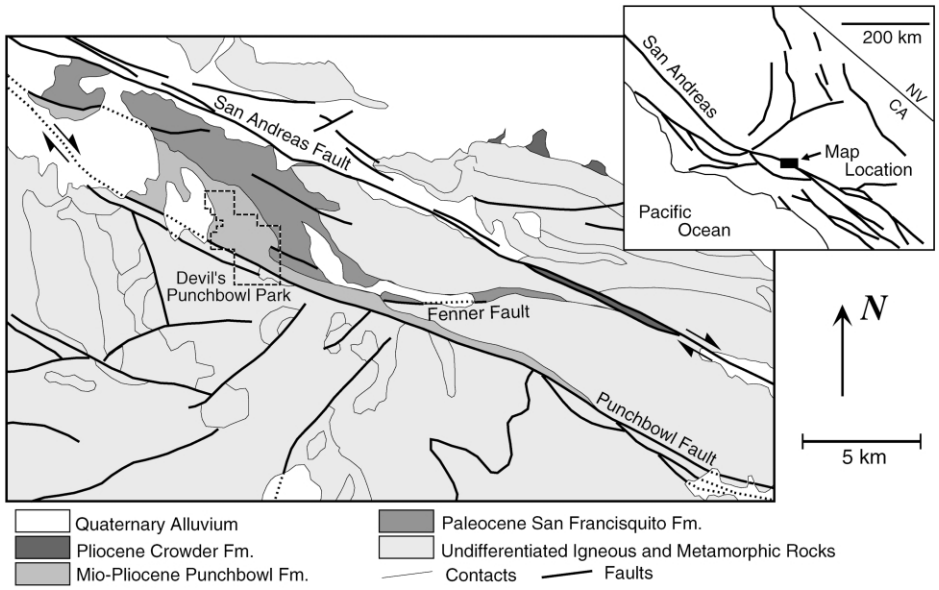

Fig. 2. Geologic map of the Punchbowl fault on the northeast side of the San Gabriel Mountains, southern California. The location of the Devil's Punchbowl Los Angeles County Park is shown.

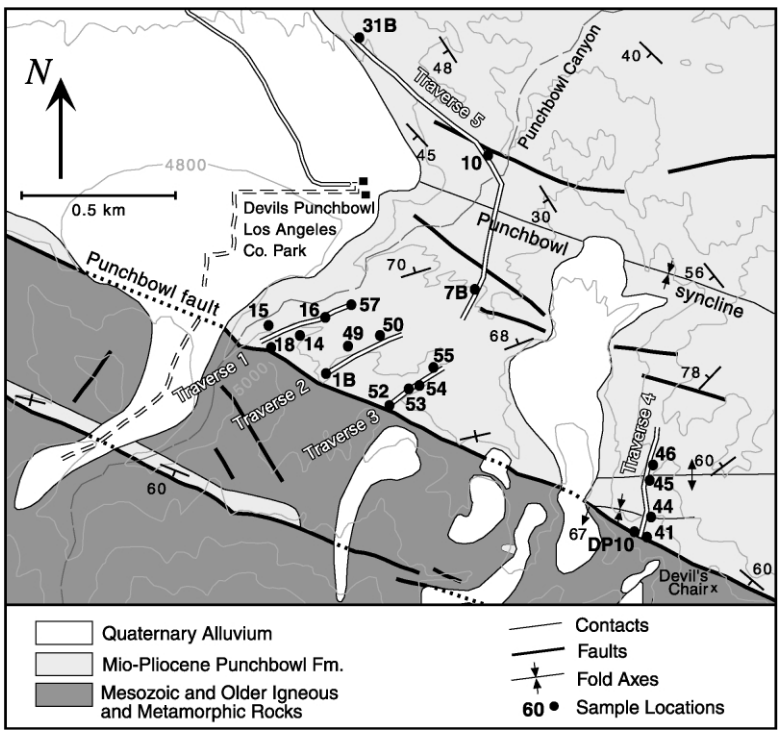

Fig. 3. Geologic map of the Devil's Punchbowl showing the sampling locations along several traverses away from the Punchbowl fault and across axes of folds in the Punchbowl Formation.

phases of Punchbowl faulting in the Middle Miocene. It is greater than 1 km thick and is composed of a basal breccia overlain by an interbedded sequence of cobbly to pebbly arkosic sandstone and siltstone (Noble, 1954; Woodburne, 1975). The basal breccia may record sedimentation associated with the fault-controlled margin of the basin (Weldon et al., 1993). The breccia both overlies and is cut by subsidiary faults of the Punchbowl system suggesting that deposition and faulting were contemporaneous (Chester, unpublished mapping, 1995). The depth of faulting recorded in outcrops of the Punchbowl fault is approximately 2–4 km (Chester and Logan, 1986). These conditions correspond to temperatures and overburden pressures of 75–125° and 22–45 MPa, respectively, and favor deformation by cataclasis with minor pressure solution (Chester and Logan, 1986).

The ultracataclasite layer of the Punchbowl fault (northern strand) is contained within a meters-thick core of highly deformed rock that displays reoriented host-rock fabric, cataclastic foliations, extreme comminution, and mineral alteration (Chester and Logan, 1986; Chester et al., 2003). Displacement on the fault was largely localized to the ultracataclasite layer of the fault core (Chester and Chester, 1998; Chester et al., 2003). Within the broader zone of damage about the core, deformation consists of folding and subsidiary faulting. Small subsidiary faults up to several meters in length are present throughout the region but are particularly numerous in the damage zone. The density of subsidiary faults in the Punchbowl Formation decreases progressively away from the core of the fault to low, regional background levels at about 30 m from the ultracataclasite (Fig. 4).

Subsidiary faults cutting the Punchbowl Formation and basement complex in the damage zone of the Punchbowl fault display preferred orientations (Fig. 5). Most faults are nearly vertical and display a single preferred orientation of *b*-axes steeply plunging to the west-northwest. Faults striking northwest are right-lateral, and faults striking

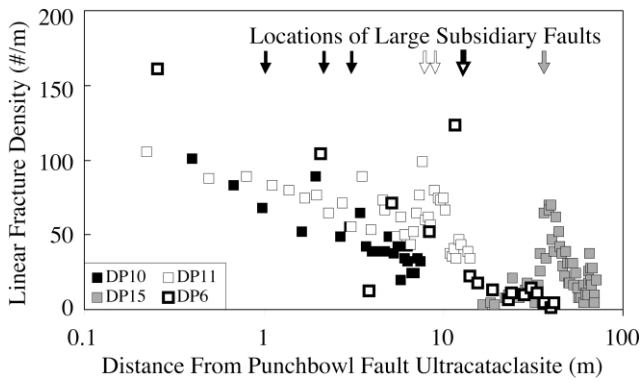

Fig. 4. Density of mesoscopic scale fractures and subsidiary faults in the Punchbowl Formation sandstone as a function of distance from the Punchbowl fault along four different traverses. Linear density is determined from the total number of fracture intercepts with two perpendicular line segments at each measurement station. Fracture density decreases with distance from the fault except locally near large subsidiary faults (shown by arrows coded to traverse by shade).

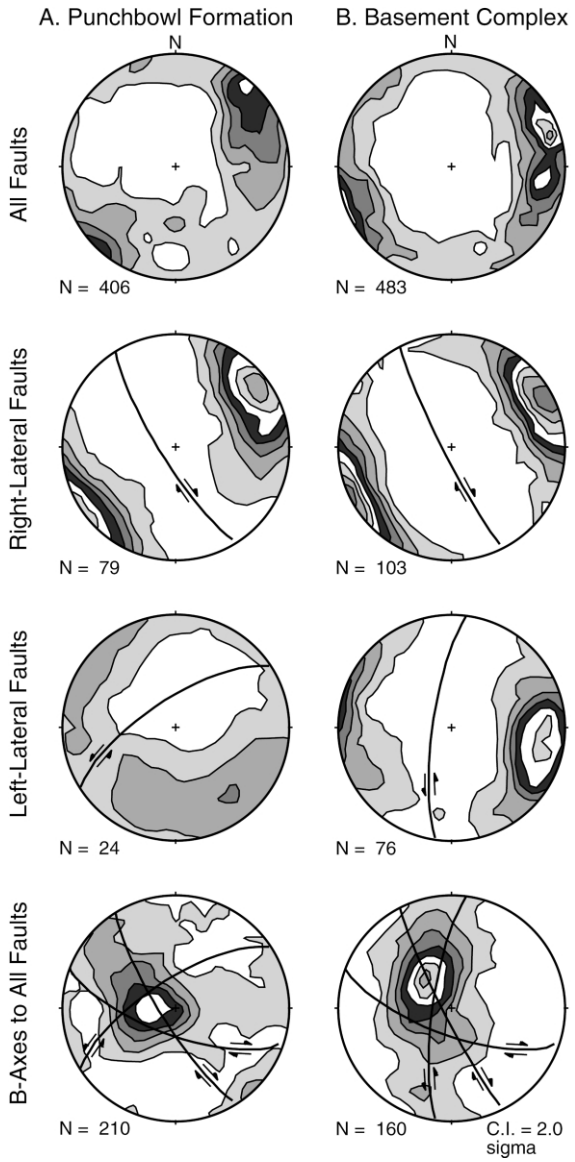

Fig. 5. Subsidiary fault fabric in the Punchbowl fault zone in the (A) Punchbowl Formation and (B) San Gabriel basement complex. Contoured fabric diagrams show normals to all subsidiary faults, normals to all faults with known right-lateral sense of shear, normals to all faults with known left-lateral sense of shear, and *b*-axes. Great circles show orientation of the Punchbowl fault and the mean orientation of right-lateral and left-lateral subsidiary faults. Lower-hemisphere equal-area projections with N at top. Number of data indicated. Contoured using Kamb method with two sigma contour interval.

north-northeast are left-lateral. The left-lateral and right-lateral subsidiary fault sets are mutually offsetting and record several episodes of deformation followed by cementation (Chester and Logan, 1986). Overall, the subsidiary faults define a quasi-conjugate geometry that reflects contraction at high angles to the Punchbowl fault (Chester and Logan, 1987). The fault-normal contraction implied by the subsidiary fault fabric suggests that the Punchbowl fault was mechanically similar to modern faults of the San Andreas system (e.g. Zoback et al., 1987; Chester et al., 1993).

Folds in the Punchbowl Formation are asymmetric and approximately cylindrical, plunging at 69° towards 247°, and the fold axes are sub-parallel to the Punchbowl fault (Chester and Logan, 1987). The amplitude and wavelength of the folds decrease with proximity to the Punchbowl fault and a greater number of minor folds occur adjacent to the fault, indicating that the folding was related to movement on the fault (Chester and Logan, 1986). The orientation of fold axes coincides with the *b*-axes of the subsidiary faults indicating that both are compatible with the same displacement field (Chester and Logan, 1987). Comparison of the fault-slip data from various locations on folds indicates that the subsidiary fault slip-data record displacement conditions subsequent to most of the folding. Both the fold geometry and the subsidiary fault fabric suggest that the slip-direction on the Punchbowl fault plunged 30° to the southeast, consistent with reverse-oblique slip motion (Chester and Logan, 1987).

3. Method

Thirty-three oriented samples of the Punchbowl Formation sandstone were collected along five traverses at distances of 0.075 m to approximately 1 km from the ultracataclasite layer of the fault (Fig. 3; Table 1). Each traverse followed a relatively massive sandstone unit in the middle section of the Punchbowl Formation, well above the basal breccia, and crossed the axes of small folds and the large Punchbowl syncline (Fig. 3). The lithology and orientations of bedding, subsidiary faults, joints, and veins were noted at each sample location. Three oriented and mutually perpendicular petrographic sections were prepared from a subset of the samples.

Optical microscopy, microprobe, and cathodoluminescence were used to describe the type of microfractures present, distribution and orientation of microfractures, composition of cements, and timing relationships between microfracturing and cementation. Samples were analyzed using a Cameca SX 50 electron microprobe with a beam current of 9.98 nA and 15.03 kV gun potential. Elemental X-ray detection maps for silicon, potassium, sodium, and calcium were made using the microprobe to identify quartz, potassium feldspar, plagioclase feldspar, laumontite, and calcite. Backscattered electron imaging and cathodoluminescence imaging were used to identify fractures and relative timing of cementation episodes. In addition, a cold Cathode Luminescence Model 8200 Mk II attached to a Nikon Optiphot Pol microscope with a gun potential of 15 kV, ~0.01 Torr vacuum, and 300 μA beam current, was used to image carbonate cements.

Microfractures were classified as intragranular, transgranular or grain-boundary fractures, and as open, partially open, sealed (microveins), and fluid inclusion planes (FIP).

Table 1
Samples of Punchbowl Formation used for fabric analysis

Sample	Distance[a] (m)	Traverse	Rock type	Fabric domains[b]	Bedding orientation	Distance to subsidiary faults
DP10B	0.075	4	Cataclastic ss	IDZ-FC	?	cm
DP10G	0.7	4	Medium-coarse ss	IDZ-FC	075, vert	cm
DP10H	1.4	4	Medium-coarse ss	IDZ-FC	075, vert	cm
DP10I	2.5	4	Medium-coarse ss	IDZ-FC	075, vert	cm
P41A	2.5	4	Medium-coarse ss	MDZ	041, 81 NW	dm
P52A	3	3	Fine ss	MDZ	081, 81 SE	dm
P41C	5	4	Medium-coarse ss	MDZ	041, 81 NW	dm
P52B	6	3	Fine ss	MDZ	081, 81 SE	dm
P52C	10	3	Medium ss	MDZ, ODZ	081, 81 SE	dm
P18	12	1	Medium ss	MDZ, ODZ	090, 75 N	10s m
DP11I	14.2	4	Medium-coarse ss	MDZ	037, 81 NW	cm
P1B	36	2	Medium-coarse ss	ODZ, PS	068, 84 NW	dm
P54	130	3	Medium-coarse ss	ODZ, PS	078, 86 NW	m
P7B	480	5	Medium ss	ODZ, PS	075, 69 NW	m
P10	900	5	Fine-medium ss	PS	322, 52 SW	dm to m
P31B	1040	5	Coarse ss	PS	350, 36 SW	10s m

[a] Distance from the ultracataclasite layer.
[b] IDZ-FC = innermost damage zone and fault core; MDZ = middle portion of damage zone; ODZ = outer damage zone; PS = five samples across Punchbowl Syncline.

Fractures cemented by secondary minerals other than quartz are obvious using optical microscopy and are classified as sealed. Fractures in quartz grains that are healed or cemented by quartz are difficult to identify without cathodoluminescence (e.g. Milliken and Laubach, 2000), but often are marked by optically visible, planar arrays of fluid inclusions, which are classified as FIP (e.g. Smith and Evans, 1984; Laubach, 1997). Partially open fractures share characteristics of open and FIP; they may be sharp-tipped with matching sides, but along some portion of the fracture consist of a planar array of fluid inclusions. Transgranular fractures cut across two or more grains and cement, and are sharp-tipped with matching sides (e.g. Kowallis et al., 1987). Intragranular fractures lie totally within a grain (e.g. Kranz, 1983; Kowallis et al., 1987). Grain boundary fractures separate neighboring grains along their boundaries.

Microfracture density data were determined for 15 samples using a petrographic microscope with a flat stage. Data were collected from 30 evenly-spaced quartz grains encountered along a traverse across each thin section (90 grains per sample). All visible fracture types were noted in the counts. Intragranular fractures were measured only in quartz grains to avoid the influence of cleavage (e.g. Blenkinsop, 1990). Density was determined by counting the number of microfractures that intersected a line of length 1.5 times the average grain diameter of the sample (e.g. Anders and Wiltschko, 1994). At each recording site, the microscope stage was rotated an arbitrary amount in order to randomize the counting line orientation. The total number of microfracture intersections was divided by the total counting line length to determine an average linear density of microfractures.

Microfracture orientations were measured in three mutually perpendicular thin sections from each sample using an optical microscope and universal stage (e.g. Friedman, 1969). Microfracture orientations were determined in forty grains per thin section (120 grains per sample) along evenly spaced traverses across each section. Orientations of intragranular fractures were only measured in quartz, while measurements of transgranular fractures were not restricted by mineralogy. The orientation and type of every microfracture in each grain was recorded. Wilson (1999) compared this method with that of Friedman (1969), in which an average orientation was recorded for each prominent set of microfractures within a grain, and concluded that either method is an acceptable technique to define the overall microfracture fabric. The data from each section were rotated from the thin section reference frame into geographic coordinates, and contoured on an equal area, lower hemisphere projection. Orientation data were contoured using Stereonet software (Allmendinger, 1995) that uses the method of Kamb (1959), and StereoNett software (Duyster, 2000) that allows contouring of weighted data.

Several types of sampling bias may arise when measuring the orientation of a planar fabric element using a universal stage. Operator bias results from the general difficulty in observing microfractures when the universal stage is inclined (Borg et al., 1960). To reduce operator bias, careful observation at all possible inclinations is necessary (e.g. Borg et al., 1960; Anders and Wiltschko, 1994). This first bias is compounded by the fact that the field of view decreases as the inclination of the stage increases (Friedman, 1969). This reduction in observation area reduces the number of microfractures that can be seen and measured at

large stage inclinations by about one third. Based on an analysis of the frequency of microfractures measured as a function of inclination, Wilson (1999) found that an inverse cosine cubed function can be applied to the data to correct for operator bias and area bias. The correction weights microfractures measured at the highest stage inclination (45°) about three times that of microfractures measured at the lowest stage inclination (0°).

Collecting data from three mutually perpendicular sections using a universal stage tilted over the full range of inclination (0° to ±45°) allows all possible orientations of a sample to be canvassed twice, leaving no blind spots (Friedman, 1969). A third sampling bias arises, however, because four small orientation regions are sampled three times, and thus sampling is not perfectly uniform. Wilson (1999) showed that the most homogeneous sampling is achieved when the inverse cosine cubed inclination correction is applied to the data, as done herein. After this correction, the triple-sampled areas are only slightly oversampled and small regions surrounding these areas are slightly undersampled, relative to the average sampling. The non-uniform sampling should be considered when assessing preferred orientations.

A fourth possible bias may be introduced when measuring all microfractures within each grain because the number of microfractures measured per grain is highly variable. Such variability may lead to apparent preferred orientations that reflect the fracture fabric of a few heavily fractured, large grains. Each microfracture orientation in this study is weighted by the fraction of the number of microfractures measured in a given grain. For example, a microfracture orientation from a grain with only two microfractures is assigned a weighting factor of 0.5 and a microfracture orientation from a grain with 10 microfractures is assigned a weighting factor of 0.1. This grain-weighting correction ensures that every grain measured contributes equally to the total fabric (Wilson, 1999) and is consistent with the technique of Friedman (1969). Additional weighting is used when constructing composite fabric plots for two or more samples. In this case, all samples are weighted equally in the final composite plot.

4. Results

4.1. Petrology

Point-count mode determinations, based on 750 counts per sample, from four representative Punchbowl Formation samples (P52A, P18, P44, P54) yield an average modal composition of 31% quartz, 13% potassium feldspar, 35% plagioclase, 8% laumontite, and 13% clay, opaques and pore space. Quartz grains are fractured and some display patchy and undulatory extinction. Potassium feldspar grains are relatively unaltered, but commonly display growth twins and cleavage-related microfractures. Plagioclase feldspar grains are rich in sodium and are commonly altered, containing numerous mica inclusions. Grain size ranges from very fine to coarse, indicating poor sorting at the time of deposition, and grain shape varies from angular to subrounded, with an average aspect ratio of 1.2:1.

The sandstones are grain-supported with laumontite and calcite cement. Laumontite is a calcium-rich zeolite, and likely is the alteration product of plagioclase. Laumontite commonly occurs in aggregates of prismatic crystals as intergranular pore cement and fracture cement, and displays cleavage-related microfractures. Calcite occurs as intergranular pore and fracture cement in many samples. The calcite displays two levels of cathodoluminescence intensity. The distribution of calcite cement is variable within a sample and between samples, being patchy to extensive. In addition to laumontite and calcite cement, clay also is present as intergranular cement and as pseudomorphs of biotite and chlorite crystals. The distribution of clay varies between samples.

4.2. Microfractures

4.2.1. Microfracture density as a function of distance from the fault

All types of microfractures are observed in all samples. Most microfractures are intragranular or grain boundary fractures; transgranular microfractures that cut several grains also are common within 5 m of the ultracataclasite layer. On the basis of optical observations, open, FIP, and partially open microfractures account for 22.2, 61.1, and 14.4% of those measured, respectively. Sealed microfractures account for 2.3% of the microfractures. Grain boundary fractures were observed in backscatter electron images but were not quantified.

The density of microfractures is variable; fine-grained samples have a lower microfracture density than coarse-grained samples. This difference may arise because smaller grains are harder to fracture (e.g. Wong et al., 1997) and because it is easier to see fractures in larger grains than in smaller grains. In spite of this variation, there is a distinct decrease in abundance of microfractures with distance from the ultracataclasite layer. Linear density of intragranular and transgranular microfractures decreases from 69 microfractures/mm at 0.075 m to 25 microfractures/mm at 1.04 km (Fig. 6). This decrease primarily occurs within tens of meters of the ultracataclasite layer, similar to the distribution of subsidiary faults (Figs. 4 and 6), and is relatively constant with increasing distance beyond about 100 m. Assuming that the constant density at greater distances represents the regional, background level of microfracturing in the host rock, then the boundary of the damaged zone, as defined by an increase in microfracture density above background, is at least 100 m from the ultracataclasite layer. It is emphasized, however, that the extent of microfracture damage directly related to Punchbowl faulting is difficult to define precisely, and much

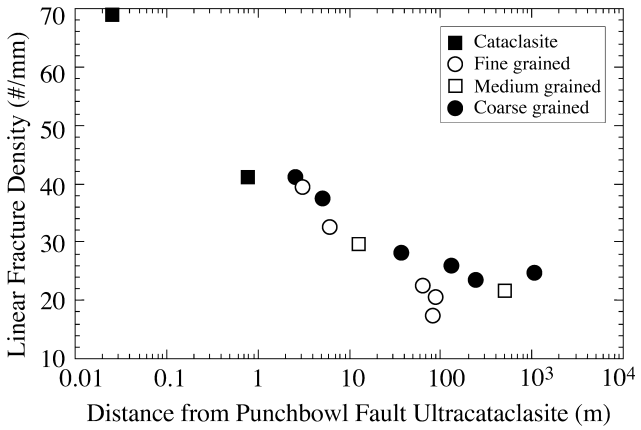

Fig. 6. Linear microfracture density in the Punchbowl Formation sandstone as a function of distance from the Punchbowl fault. Density determined from the total number of fracture intercepts along ninety (90) randomly oriented line segments from three mutually perpendicular petrographic sections for each sample.

of the regional microfracturing may have been contemporaneous with Punchbowl faulting. The majority of microfractures within 30 m of the ultracataclasite are fault related.

4.2.2. Timing of fracture and cementation

Cross-cutting relationships between different types of microfractures and cement are observed in many samples (Fig. 7). Intragranular FIP are common in the quartz grains, generally displaying planar geometries that extend partly or completely across grains. Some FIP are inherited from the parent rock and thus predate deposition of the sandstone (Fig. 7a). However, several relationships indicate many of the FIP in the Punchbowl Formation sandstone samples postdate deposition and are related to Punchbowl faulting. FIP emanating from contacts between neighboring grains, and alignment of FIP across contacts between neighboring grains indicate that many formed after deposition of the sandstone. Moreover, formation of FIP associated with Punchbowl faulting is indicated by the fact that the density of FIP increases towards the ultracataclasite layer of the Punchbowl fault similar to the total microfracture population.

Calcite and laumontite cement fills pores, as well as seals or partially seals some grain-boundary, intragranular and transgranular fractures, particularly within the damage zone of the fault (Fig. 7). In some cases, cement within intragranular microfractures connects with neighboring pore cement indicating that some microfracturing was contemporaneous or predated cementation of the sandstone (Fig. 7c and d). Calcite and laumontite sealed fractures increase in density towards the ultracataclasite layer of the Punchbowl fault, similar to the other classes of microfractures.

Evidence for timing of calcite and laumontite cementation is observed in several samples where both types of cement are present. Prismatic crystals of laumontite cement occur directly adjacent to quartz and feldspar grains, suggesting crystal growth of laumontite into open pore space. In addition, calcite cement occurs within the laumontite-lined pores, and in some cases contains fragments of laumontite crystals. Very close to the ultracataclasite layer, laumontite cement is cut by a dense network of calcite-sealed microfractures. These relations indicate that laumontite cementation largely predated calcite cementation and occurred during Punchbowl faulting.

At least two distinct episodes of calcite cementation can be distinguished on the basis of cathodoluminescence (Fig. 7e and f). In general, a weakly luminescent calcite fills pore space, and a strongly luminescent calcite is noted in pores and in transgranular and grain boundary microfractures. The strongly luminescent calcite also fills microfractures that cut through the weakly luminescent calcite cement. These relations indicate that the strongly luminescent calcite postdates the weakly luminescent calcite. The fact that both types of calcite cement are mechanically twinned suggests that both types underwent deformation associated with movement along the Punchbowl fault. More than two episodes of calcite cementation is suggested by the structure of sealed microfractures and presence of fragments of calcite-cemented fractures in the ultracataclasite layer. Calcite-sealed fractures display all degrees of shear-related disruption from undeformed, to segmented, to isolated fragments (porphyroclasts) within the ultracataclasite matrix and record repeated fracture and cementation during progressive deformation (Chester and Logan, 1987). The presence of calcite-filled fractures in the core and damage zone of the fault, the decrease in number of such fractures with distance from the fault, and the presence of disrupted calcite-cemented fractures (vein fragments) in the Punchbowl ultracataclasites (Chester and Logan, 1987) indicate that microfracturing and sealing by calcite was contemporaneous with slip on the fault.

4.2.3. Microfracture orientations

The orientations of microfractures (i.e. open, partially open, sealed, and FIP) within individual samples vary from nearly random to markedly non-random. When samples are analyzed as a function of distance from the ultracataclasite layer, the microfractures in each group display preferred orientations (Fig. 8).

Sample DP10B represents a cataclastic sandstone of the Punchbowl fault core taken several centimeters from the boundary of the ultracataclasite layer (Table 1). This sample contains extensive calcite cement sealing intragranular and transgranular microfractures. The open and sealed microfractures display the strongest preferred orientations; the dominant set is composed of sealed, steeply dipping, northwest striking microfractures that form an acute angle with the Punchbowl fault (Fig. 8). Additional sets include northwest striking, vertical, open microfractures; northwest striking, southwest dipping sealed microfractures; and vertical sealed microfractures that are approximately

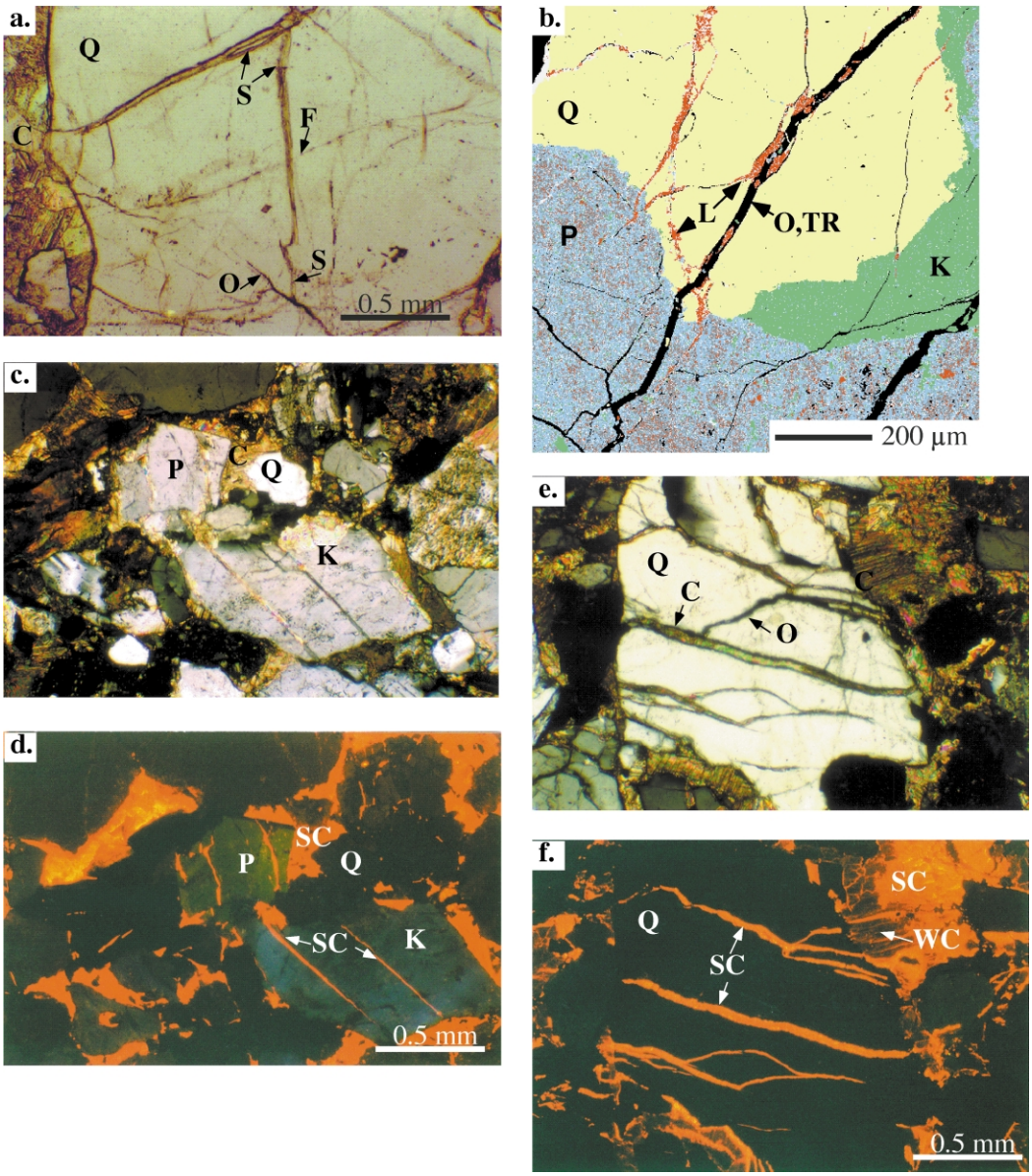

Fig. 7. (a) Photomicrograph of open microfractures, sealed microfractures, and FIP in a quartz grain. Open microfractures cut sealed microfractures and sealed microfractures cut FIP. Q = quartz, C = calcite cement, O = open microfracture, F = fluid inclusion planes, and S = sealed microfracture. Plane-polarized light. (b) False color X-ray elemental image of large open transgranular microfracture (O, TR), cutting laumontite-sealed microfractures (L). Q (yellow) = quartz, P (blue) = plagioclase feldspar, K (green) = potassium feldspar, L (red) = laumontite. (c) Transmitted, cross-polarized light and (d) cathodoluminescence image of intragranular microfractures filled with calcite. The calcite in microfractures and pores appears similar in cathodoluminescence intensity. SC = strongly luminescent calcite. (e) Transmitted, cross-polarized and (f) cathodoluminescence image of strongly and weakly luminescent calcite in pores and microfractures. Strongly luminescent calcite cuts weak luminescent calcite. Q = quartz, SC = strongly luminescent calcite, and WC = weakly luminescent calcite.

perpendicular to the Punchbowl fault. The partially open microfractures and FIP have more random orientations, but still display weak preferred orientations that are similar to those of the open and sealed microfractures.

Samples DP10G, DP10H, and DP10I represent the heavily fractured and faulted sandstone that is located at 0.7–2.5 m from the ultracataclasite layer (Table 1). The microfractures in these samples display similar fabrics and a distinct preferred orientation (Fig. 8). The normal to open microfractures and FIP define a girdle with two broad point maxima. One maximum represents northwest striking microfractures that are steeply dipping to the northeast. This set is similar in orientation to the open and sealed fractures in sample DP10B. The other maximum consists of microfractures oriented approximately perpendicular to the Punchbowl fault with subhorizontal to northwest dips.

Open and partially open microfractures and FIP in samples taken at 2.5 m (P41A) and 3.0 m (P52A) from the ultracataclasite along traverses 3 and 4 (Table 1) display preferred orientations (Fig. 8). In all cases, the preferred

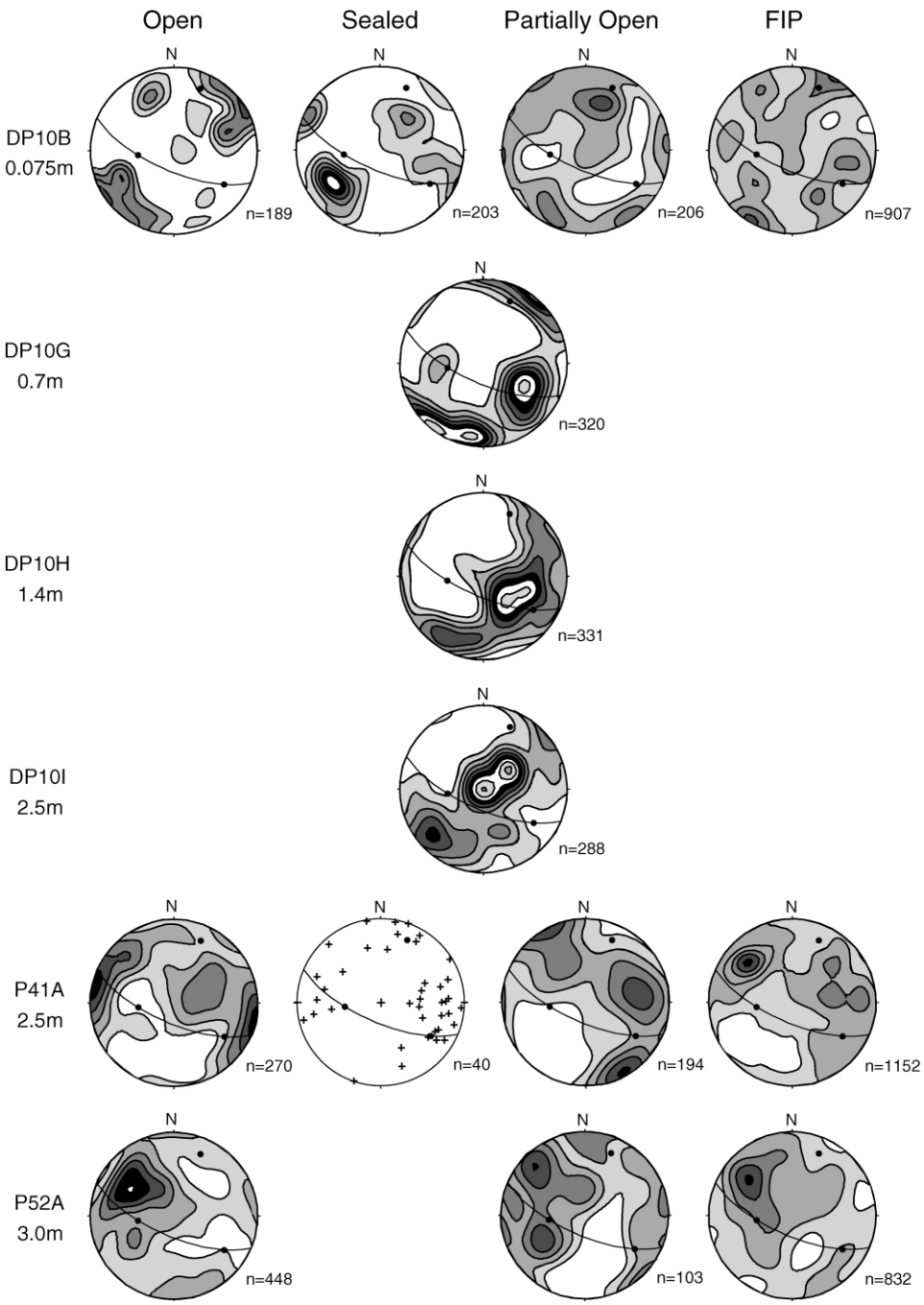

Fig. 8. Fabric of open, sealed, and partially open microfractures, and FIP within individual samples. Great circle shows orientation of the Punchbowl fault; filled circles show the orientation of the Punchbowl fault *b*-axis, normal and slip direction. Lower-hemisphere equal-area projections with N at top. Density contour interval is one sigma beginning with two sigma. Number of data indicated.

orientation is approximately perpendicular to the Punchbowl fault and vertical to steeply dipping. The microfracture sets at acute angles to the Punchbowl fault, seen in the samples closer to the ultracataclasite layer (DP10G, DP10H, DP10I), are not present at 2.5 m from the ultracataclasite layer.

Samples P41C, P52B, P52C, P18, and DP11I, taken between 5 and 14.2 m from the ultracataclasite layer, were collected along three different traverses across the damage zone of the Punchbowl fault (Table 1). Within each sample, the orientations of open, partially open, and sealed microfractures, and FIP are similar (Fig. 8). In addition, the fabrics of the five different samples are similar. Overall, this common fabric is characterized by a single preferred orientation that strikes approximately perpendicular to the Punchbowl fault and dips steeply to the northwest. This

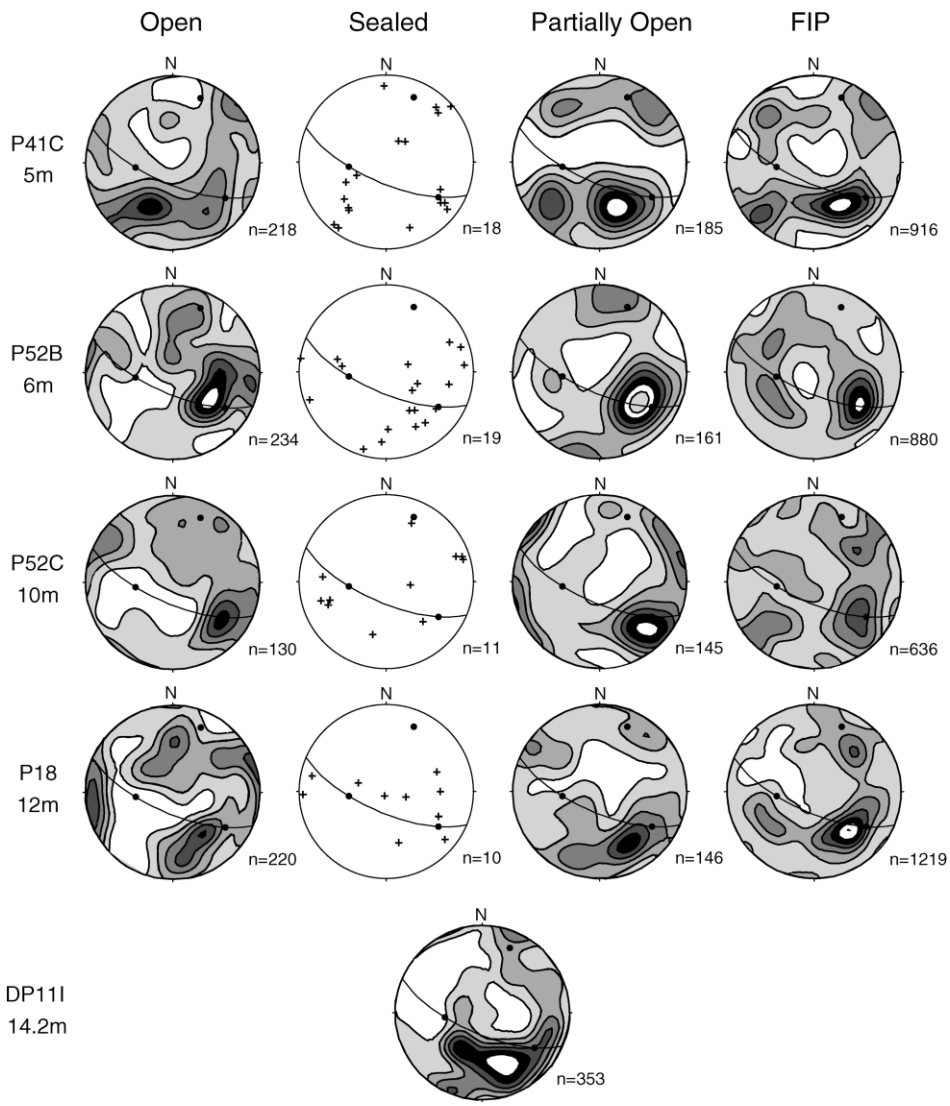

Fig. 8 (*continued*)

preferred orientation is similar to one of the fracture sets developed close to the ultracataclasite layer (samples DP10G, 10H, and 10I). In fact, all the samples between a distance of 0.7 and 14.2 m display a set of microfractures that is nearly perpendicular to the Punchbowl fault, though the magnitude and direction of dip is somewhat variable.

The remaining samples (P1B, P54, P7B, P10, P31B) represent damage at 36–1040 m from the ultracataclasite layer (Table 1). Microfractures in these samples display one or more sets with moderate to weak preferred orientations (Fig. 8). Some of the samples display preferred orientations similar to those of samples closer to the ultracataclasite layer. Relative to the samples closer to the fault, however, there is much less similarity in orientation when the different types of microfractures within a sample are compared, and in orientation of a particular type of microfracture when data from different samples are combined.

5. Discussion

5.1. Spatial and temporal analysis of microfracture fabric

Sampling along several traverses achieves spatial coverage both parallel and perpendicular to the fault trace (Fig. 3; Table 1). Grouping samples by distance from the ultracataclasite layer allows us to define several fabric domains that are characterized by relatively homogeneous preferred orientations (Table 1). In the discussion below we explore whether these fabric domains correspond to previously defined structural zones of the fault: the fault core, damage zone and undeformed host rock (e.g. Chester and Logan, 1986; Chester et al., 1993). In addition, we consider the fabric of the different types of microfractures within each spatial domain to investigate fabric evolution. It was not possible to determine the relative age of most microfractures used for orientation analysis, however, based on

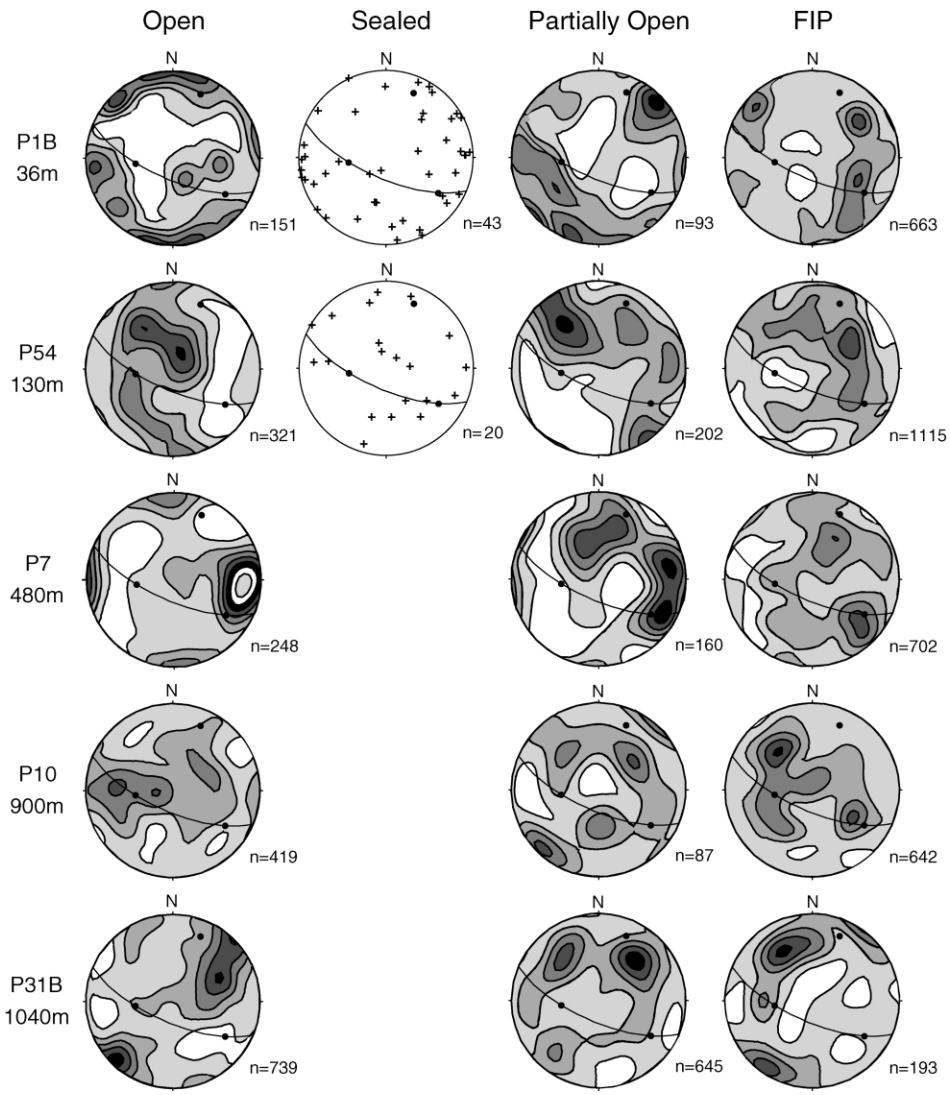

Fig. 8 (*continued*)

cross-cutting relations between microfractures and cements, and between the different types of cement, we infer that the FIP are the most ancient microfractures, and thus record the earliest fracturing events. It is possible that some FIP are inherited from the parent rock and therefore represent fracture events unrelated to Punchbowl faulting. Nonetheless, because the density of FIP increases towards the fault and orientations within each spatial domain are similar to the other fracture types, we conclude that the preferred orientations of the FIP are representative of fracturing during the growth of and subsequent wear along the Punchbowl fault. The open fractures, in general, cut all other fracture types and are interpreted to record the latest fracturing events. Open microfractures are the most likely fracture type to record post-faulting processes, such as uplift and exhumation (Fig. 9), as well as damage during sample preparation. However, the density, fabric and cross-cutting relations of the open fractures suggest that they were formed during the faulting process, and thus are used as a record of deformation during later stages of faulting. The partially open and sealed microfractures are used as the best record of intermediate-stage fracture events (Fig. 9).

5.1.1. Middle damage zone (MDZ) fabric domain

The microfracture orientations recorded in seven samples between 2.5 and 14.2 m of the ultracataclasite layer display a similar orientation that is nearly normal to the Punchbowl fault. These microfractures define a distinct fabric domain (Fig. 8). Composite plots of the microfractures within this zone, distinguished on the basis of type, illustrate that the (a) dominant preferred orientation for all types, and therefore all time periods, is similar, (b) average microfracture orientation is approximately perpendicular to the inferred slip vector of the fault, and (c) preferred orientation is strongest for the oldest and intermediate time

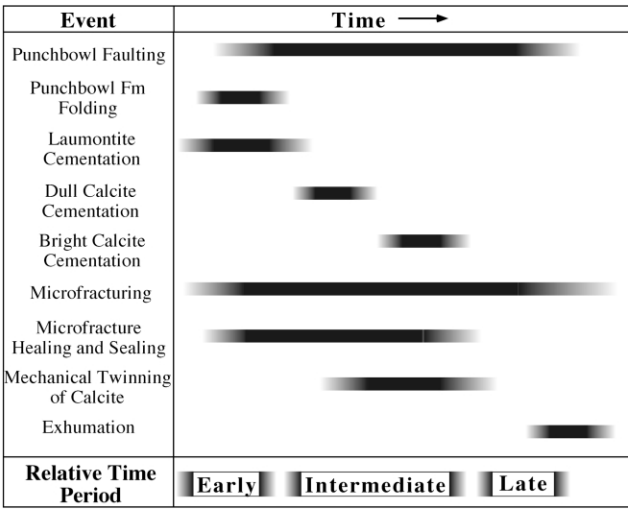

Fig. 9. Relative timing of events related to Punchbowl faulting in the Devil's Punchbowl area inferred from timing determinations as described in text. The early, intermediate and late relative time periods recorded by the fabrics of FIP, partially open and sealed microfractures, and open microfractures, respectively, are indicated.

periods, and weakest for the most recent time period (Fig. 10).

On the basis of microfracture (Fig. 6) and subsidiary fault (Fig. 4) densities, the 2.5–14.2 m interval covered by these samples occurs in the middle portion of the damage zone of the Punchbowl fault (Fig. 3). The preferred orientation of microfractures in this domain bisects the quasi-conjugate set of subsidiary faults cutting the damage zone (Fig. 5a). In addition, the line of intersection of the average microfracture orientation and the plane of the Punchbowl fault is approximately colinear with the average orientation of *b*-axes defined by the subsidiary faults and with the axes of the folds in the Punchbowl Formation (Fig. 10). These data illustrate that the microfracture fabric is consistent with the displacement field of the Punchbowl fault and Punchbowl Formation folds. The microfracture fabric also is consistent with the inferred paleostress field implied by the conjugate geometry of the subsidiary faults, in which the maximum principal compressive stress is approximately normal to the Punchbowl fault and the minimum principal compressive stress is approximately parallel to the slip direction of the Punchbowl fault. The microfracture fabric of the MDZ suggests that the kinematics of Punchbowl faulting, as well as the spatial and temporal average orientation of principal paleostress axes within the damage zone were the same during the early, intermediate and late periods of Punchbowl fault history.

5.1.2. Inner damage zone and fault core (IDZ-FC) fabric domain

The microfracture orientations recorded in the four samples taken from within 2.5 m of the ultracataclasite layer constitute a second fabric domain (region of DP10; Fig. 3) displaying two distinct preferred orientations (Fig. 8).

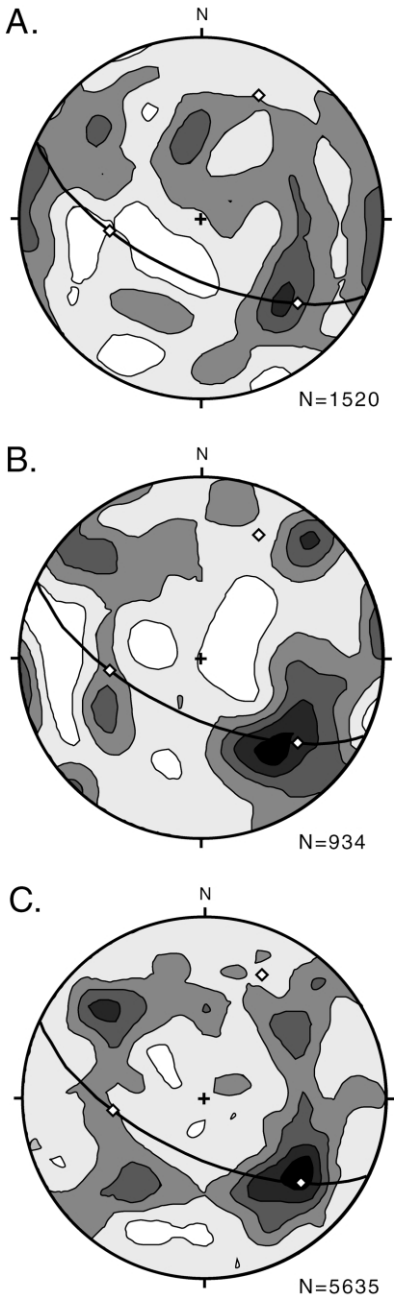

Fig. 10. Contour diagrams of composite fabrics for (A) open microfractures, (B) partially open microfractures, and (C) FIP in the middle portion of the damage zone (MDZ). Great circle shows orientation of the Punchbowl fault; diamonds show the orientation of the Punchbowl fault *b*-axis, normal and slip direction. Lower-hemisphere equal-area projections with N at top. Density contour interval is one sigma beginning with two sigma. Number of data indicated.

On the basis of microfracture and subsidiary fault densities (Figs. 4 and 6), and the extent of mesoscopic scale shearing evident at DP10, the three samples between 0.7 and 2.5 m from the ultracataclasite are from the innermost damage zone (IDZ). Sample DP10B, at 0.075 m from the ultracataclasite layer, represents a cataclasite from the fault core (FC).

Microfracture orientations in samples from the (IDZ)

display two distinct fracture sets. One set is at a very high angle to the Punchbowl fault, similar to the preferred orientation of microfractures in the MDZ (Figs. 8 and 10). The second set strikes approximately parallel to the Punchbowl fault, but dips steeply to the northeast, about 30° from the plane of the Punchbowl fault. This second set of microfractures also is evident in the open and sealed microfractures of the fault core sample, DP10B (Fig. 8).

The fact that the average orientation of open and sealed microfractures at DP10B is not evident in the FIP and partially open microfractures is most simply explained by shear-induced disruption of the more ancient fabrics. Sample DP10B is a calcite-cemented cataclasite. Clastic particles of quartz and feldspar are highly fractured and disaggregated, and the amount and distribution of calcite cement records significant dilation. On the basis of timing relations, it appears that the sample underwent grain-scale cataclastic flow prior to and during the early phases of calcite cementation. Shear by cataclastic flow is expected to disrupt and randomize the earlier formed FIP and partially open microfractures. After calcite cementation, the grain-scale cataclastic flow became less significant, and the cataclastic texture was overprinted by a system of sealed and open microfractures that display a preferred orientation.

The microfracture fabric of samples from the IDZ-FC fabric domain suggests that the single preferred orientation of microfractures present in the MDZ extends throughout the entire damage zone up to the boundary with the cataclasite of the fault core. It appears that the second set of microfractures, noted in the cataclasite of the fault core, also occurs in the innermost portion of the damage zone. Similar to the fabric of the MDZ, both of these sets appear to have been formed during the early, intermediate, and late stages of Punchbowl faulting, though the early stage fabrics within the fault core were disrupted by grain-scale cataclasis.

5.2. Timing of folding relative to microfracture fabric development

The samples used for microfracture fabric analysis were collected along several traverses through folded Punchbowl Formation strata (Fig. 3). Clearly, the strata underwent rotations associated with folding. In order to use the microfracture fabrics to test models for fault damage development, it is necessary to define the relative timing of folding and microfracture fabric development, and to determine if microfracture fabrics have been reoriented by folding since formation.

To determine the relative timing of microfracture fabric formation and folding we compare the fabrics of a suite of samples collected from different locations in folded strata. If samples taken from strata with different bedding orientations show the same preferred orientation of microfractures in the present state, it is likely that the folds formed before the development of the preferred orientation. In contrast, if unfolding strata brings the microfracture orientations into coincidence, then the fabric likely developed prior to folding or is related to folding.

To explore the relation between folding and microfracture fabric development, the FIP from two domains are rotated to the pre-fold orientation as the strata are unfolded. To unfold the strata we use an average fold axis orientation and the bedding orientation at each sample location. First, the fold axis is rotated to horizontal about a horizontal rotation axis, and second, the strata are rotated to horizontal about the strike-line. We concentrate on the FIP because they are the most likely to record the development of an early, pre-folding fabric. In the MDZ, microfracture data were measured in strata having bedding orientations that vary up to 50° in strike and 20° in dip (Figs. 8 and 10; Table 1). We find that unfolding the strata tends to randomize the composite fabric of FIP relative to the present-day fabric (Figs. 10C and 11A). This result suggests that the folding occurred prior to significant development of the preferred orientations noted in this domain.

The orientation of bedding varies 166° in strike and 50° in dip for the five samples taken at distances greater than

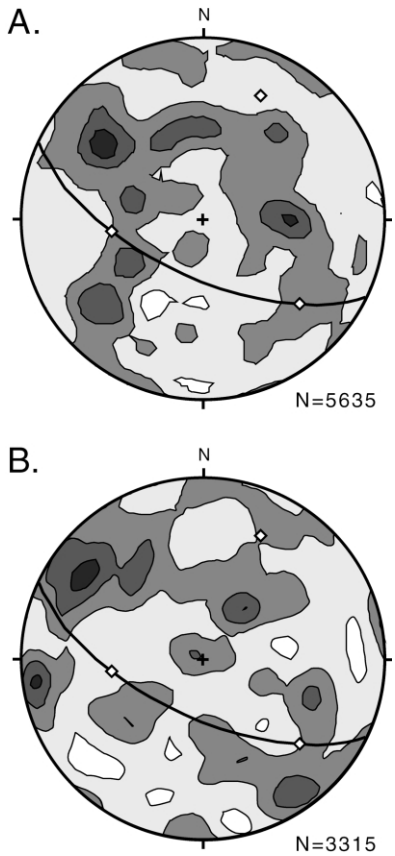

Fig. 11. Composite fabric of FIP rotated to the pre-fold orientation for the (A) middle portion of the damage zone (MDZ) and (B) five samples from the limbs of the Punchbowl syncline furthest from the ultracataclasite layer. Compared with the present day fabrics in the MDZ (Fig. 10C) and in the samples from the limbs of the Punchbowl Syncline, the prefolding fabrics are more random (see text). Symbols are the same as in Fig. 10. Lower-hemisphere equal-area projections with N at top. Density contour interval is one sigma beginning with two sigma. Number of data indicated.

35 m from the ultracataclasite layer and across the Punchbowl syncline (Table 1). Although each microfracture type displays a preferred orientation in these samples, there is little spatial or temporal consistency between sample fabrics (Fig. 8c). Considering again the composite fabric of the FIP, we find no significant increase in preferred orientation of microfractures if the fractures are rotated to a pre-fold geometry (Fig. 11b).

5.3. Origin of microfractures in the damage zone

The distribution of microfractures documented in this study, specifically the observation that the density of microfractures decreases monotonically with the logarithm of distance from the fault (Fig. 6), is consistent with observations of damage about other fault zones (e.g. Scholz et al., 1993; Anders and Wiltschko, 1994; Moore and Lockner, 1995; Vermilye and Scholz, 1998; Chester et al., 2003). Most of these previous studies document the density distribution of microfractures in the tip regions of natural, small-displacement faults (e.g. Vermilye and Scholz, 1998) or those produced in the laboratory (Moore and Lockner, 1995). Observations suggest that a log-distance distribution of damage along a well-established fault also could reflect the early stages of deformation associated with fault formation and tip propagation (e.g. Cowie and Scholz, 1992; Scholz et al., 1993). If true, the timing of microfracture fabric development and the distribution of microfracture orientations in the damage zone should reflect the processes of fault formation. To investigate this possibility, we compare the microfracture fabric for the Punchbowl fault with the fabrics predicted on the basis of mechanical models of fault formation and wear. To facilitate the comparison, we show the microfracture orientations predicted by models for a fault with the orientation, sense of shear, and slip direction appropriate for the Punchbowl fault (Fig. 12). For all models, the normal to the average microfracture orientation (the minimum principal compressive stress direction) should lie in the plane containing the Punchbowl fault slip vector and the normal to the Punchbowl fault surface. The direction of the normal within this plane will be different for each model. Model predictions are shown on contoured plots of the composite microfracture data for the IDZ-FC and MDZ domains (Fig. 13).

The Andersonian model of faulting is based on a homogeneous stress state and Coulomb failure criteria. This model predicts that the maximum principal compressive stress is approximately 30° to the plane of a fault (e.g. Anderson, 1942; Scholz, 1990). For such a model, normal to the microfractures will be oriented at 30° to the fault normals, in the direction of the slip vector (Figs. 12 and 13). In contrast, models of fault growth that recognize heterogeneous stress distributions (i.e. local stress concentrations and a reorientation of stresses) during tip propagation and linkage of segments predict that microfractures form early

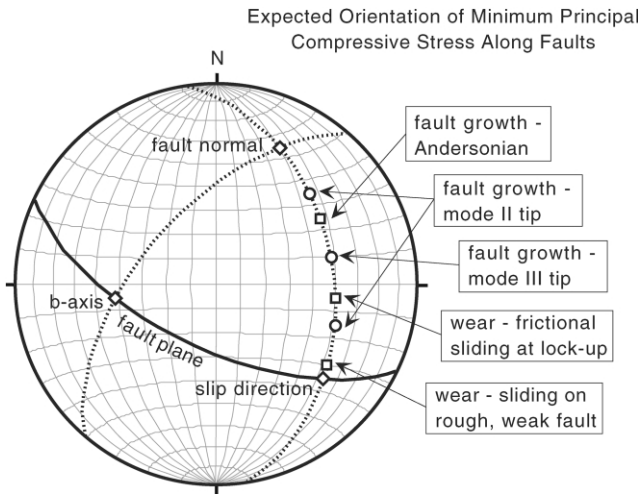

Fig. 12. Orientations of microfractures predicted by models of fault growth and wear for the Punchbowl fault. Great circle shows orientation of the Punchbowl fault; diamonds show the orientation of the Punchbowl fault *b*-axis, normal and slip direction assuming a N65°W strike, 65°SW dip, and 35° rake to the SE. Lower-hemisphere equal-area projections with N at top.

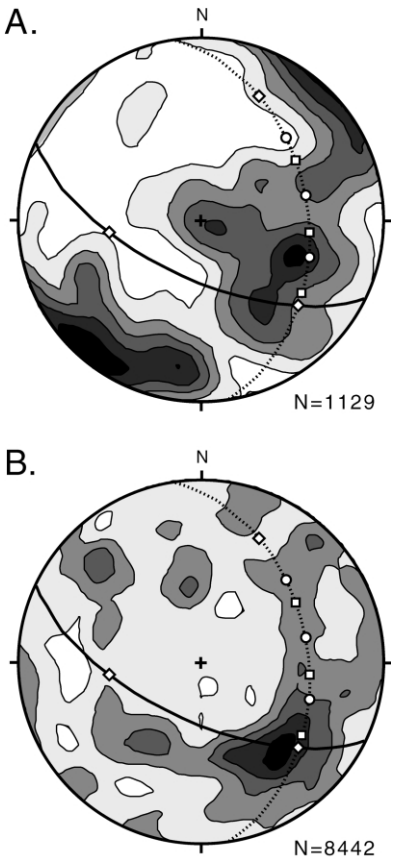

Fig. 13. Comparison of fault model predictions and the composite fabric of all microfracture types in the (A) inner damage zone and fault core (IDZ-FC) domain, and (B) for the middle portion of the damage zone (MDZ) domain. Symbols the same as in Fig. 12. Lower-hemisphere equal-area projections with N at top. Number of data indicated.

in fault history and should form in several distinct orientations. On the basis of elastic models of crack-tip stress, the predicted angle between fractures located in the wake of a propagating mode II tip and the master fault is 20° to the fault surface on the compressional side, and 70° on the tensile side (e.g. Scholz et al., 1993). The expected angle between microfractures at a mode III tip and the fault surface is 45° (Figs. 12 and 13). The fact that microfractures throughout the MDZ of the Punchbowl fault display a single preferred orientation that is approximately normal to the Punchbowl fault indicates that neither of the above models fit the observed data. The fabric of the IDZ-FC does not compare favorably with the predictions of the Andersonian model (Fig. 13). When considering tip-propagation models, we find that the high-angle microfracture set of the IDZ-FC is consistent with one orientation predicted for mode-II tip propagation. However, the low-angle set is not compatible with any tip-propagation prediction.

Observations that the preferred orientation of microfractures remained the same throughout Punchbowl fault activity are consistent with models of wear that assume progressive accumulation of microfracture damage during sliding on an established fault surface. Frictional sliding on a fault can occur under a wide range of stress orientations. Assuming homogeneous stress and typical friction coefficients for rock ($\sim$0.7), the maximum principal compressive stress may be oriented up to 65° before a fault will lock (e.g. Sibson, 1995). If a fault experiences weakening and a reduction in friction, as has been proposed for faults of the San Andreas system, then the maximum principal compressive stress may be oriented at even greater angles to the fault surface and still produce frictional sliding (e.g. Zoback et al., 1987; Fig. 12). Microfractures in the MDZ are approximately perpendicular to the fault, which suggests that the maximum principal compressive stress was perpendicular to the fault, and that the resolved shear stress on the fault surface was nearly zero. Frictional slip under such a stress orientation would be impossible if a homogeneous stress state is assumed. On the basis of the preferred orientation, timing, and density distribution of microfractures, we infer that the processes leading to microfracture damage reflect heterogeneous local stress states along the fault surface associated with slip rather than a homogeneous stress state and the far-field stress driving the fault.

Local stress concentrations along a fault can result from gradients in slip magnitude and from slip on geometrically irregular (rough) surfaces. Mechanical modeling of stress and deformation about a wavy frictional fault surface indicates that stress is heterogeneous due to the juxtaposition of geometric irregularities (Chester and Chester, 2000). For elastic properties and a fault geometry appropriate to crustal faults, the local normal stress and shear stress along and across a fault will vary in magnitude. For the case of a frictional fault, inelastic deformation (failure) is expected to occur locally in the wall rock near the fault surface. Within the predicted regions of failure, the orientation of the local maximum principal compressive stress is different from that of the far-field stress, particularly for a fault with a relatively low coefficient of friction (e.g. Saucier et al., 1992; Chester and Fletcher, 1997; Chester and Chester, 2000). Under some loading conditions, the maximum principal compressive stress is oriented nearly normal to the fault surface in regions undergoing inelastic failure near the fault surface. With continued displacement on a fault surface, wall rock should undergo stress cycling associated with repeated juxtaposition of different roughness elements at all scales. Such stress cycling would lead to the repeated failure of the wall rock throughout the lifetime of the fault. The microfracture fabric displayed in the MDZ of the Punchbowl fault is compatible with the mechanical model for wear along a fault surface (Figs. 12 and 13).

The microfracture fabric of the IDZ-FC also is compatible, in a general sense, with stress concentrations associated with sliding on a rough surface. Mechanical models predict that stress directions and magnitudes vary greatly near a nonplanar fault surface, particularly when the surface has a relatively low coefficient of friction (e.g. Saucier et al., 1992; Chester and Fletcher, 1997; Chester and Chester, 2000). As a result, fractures oriented normal to the fault surface may form locally along the surface, as well as throughout the damage zone. However, mechanical analyses also indicate that the magnitude of normal stress very close to or at the fault surface can approach zero. Low normal stress along portions of the surface could lead to separation of the surface and generation of microfractures oriented at low angles to the surface (Fig. 1c). Thus wear along a rough surface may explain the observations of microfracture orientations at both low and high angles to the fault in the IDZ-FC (Fig. 13).

Although there is no direct evidence that the Punchbowl fault was seismic, it likely was the site of numerous earthquake slip events based on analogy with other large faults of the San Andreas system in southern California (e.g. Chester et al., 2003). Stress concentration associated with the passage of an earthquake rupture tip must be considered a potential cause for wear along established faults that may contribute to accumulation of microfracture damage (e.g. Scholz et al., 1993). The microfractures produced at an earthquake rupture tip are expected to have the same orientation as those formed during fault growth by tip propagation, although the region about the tip undergoing microfracture may be considerably smaller than during fault growth (e.g. Cowie and Scholz, 1992). The microfracture sets within the IDZ-FC are oriented at both low and high angles to the Punchbowl fault as expected for mode II tip stress. However, the low angle microfractures are not perfectly compatible because the normal to the low-angle microfracture set lies out of the plane containing the normal to the Punchbowl fault and the Punchbowl fault slip vector (Figs. 12 and 13). It is possible that the IDZ-FC fabric does reflect localized microfracturing associated with earthquake rupture-tip stress concentration, and the lack of perfect

alignment is due to a late-stage rotation of strata at location DP10 associated with subsidiary faulting, block rotation, and minor folding. Better documentation of the along-strike homogeneity and average preferred orientations of microfractures in the IDZ-FC domain is needed to test this possibility.

5.4. Formation of the Punchbowl fault and weakening with displacement

Characterization of the displacement distribution in the core of the Punchbowl fault through detailed mapping suggests that almost all of the slip on the fault occurred in the ultracataclasite layer (Chester and Chester, 1998; Chester et al., 2003). It follows that the extreme localization of slip and establishment of a through-going master fault surface must have occurred very early in Punchbowl faulting history. If the microfracture damage documented in this study primarily was produced throughout the accumulation of displacement, one may not expect to observe a fabric that reflects fault formation and initial localization in the damage zone. If the extreme localization of slip on the Punchbowl fault records a weakening of the fault with displacement (e.g. Chester et al., 1993), then the damage also may have progressively focused about the fault surface. If true, the earliest record of fabric development is most likely preserved by the most ancient microfractures in the outermost damage zone of the fault where overprinting by wear processes would be minimized.

Inspection of the fabric of FIP in samples at distances from the ultracataclasite ranging between 10 and 480 m show evidence of a spatially homogeneous fabric (Fig. 8). On the basis of microfracture intensity traverse data, the sample interval between 10 and 480 m would cover the outermost damage zone (ODZ) and boundary with the undeformed host rock (Fig. 6). The FIP fabric in the ODZ displays two sets, as shown by the composite fabric diagram for the six samples (Fig. 14). One set is perpendicular to the Punchbowl fault as seen throughout the damage zone. The other set is at an angle of approximately 30° to the Punchbowl fault, consistent with the orientation predicted by the Andersonian fault model. This second set of microfractures may record the orientation of the minimum principal compressive stress during the early stages of fault formation. Because these samples come from folded strata, this microfracture fabric also must postdate the folding of the Punchbowl Formation.

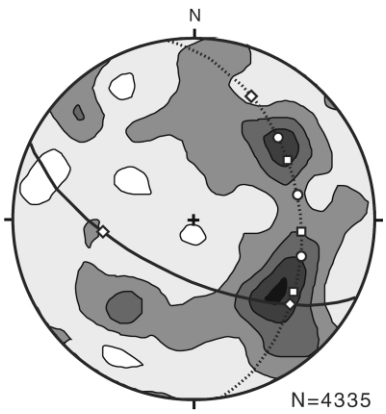

Fig. 14. Comparison of fault model predictions and the composite fabric of all FIP in the outer portion of the damage zone (ODZ) domain. Symbols the same as in Fig. 12. Lower-hemisphere equal-area projections with N at top. Number of data indicated.

Sealed microfractures and FIP observed in oriented core recovered from 0.5 to 1.7 km depth in the Cajon Pass drill hole near the San Andreas fault also display preferred orientations (Blenkinsop, 1990; Wang and Sun, 1990; Blenkinsop and Sibson, 1992). Based on existing data, the timing of microfracturing remains inconclusive (Blenkinsop, 1990; Wang and Sun, 1990; Blenkinsop and Sibson, 1992); however, it is important to note that one set is perpendicular to the San Andreas fault. The drill hole is approximately 4 km from the right-lateral San Andreas fault, and within 1 km of the Squaw Peak thrust and left-lateral Cleghorn faults (Blenkinsop, 1990; Wang and Sun, 1990), therefore it is uncertain whether all microfractures observed in the drill hole reflect damage associated only with San Andreas faulting.

A kinematic history for deformation of the Punchbowl Formation associated with Punchbowl faulting that is compatible with the structural data and timing observations is as follows. Initial deformation involved folding of the strata as the Punchbowl fault began to propagate through the Punchbowl basin deposits, possibly analogous to forced folding above blind, oblique-slip basement faults. As folds tightened and locked, a pervasive microfracture fabric developed up to ~500 m from the fault surface in response to the early stress state during propagation and localization of the Punchbowl fault in the Punchbowl strata. This early phase of deformation may, in part, be recorded in the ODZ by the FIP that have orientations consistent with the Andersonian model of faulting. After the through-going Punchbowl fault was established, progressive weakening and focusing of damage with displacement occurred. During this time period, the microfracture fabric in the damage zone developed in response to stress cycling as surface irregularities were repeatedly juxtaposed during slip events. The stress concentration associated with the passing of earthquake rupture tips may have contributed to the fabric of the IDZ-FC domain adjacent to the ultracataclasite layer.

6. Conclusions

The Punchbowl Formation sandstone adjacent to the Punchbowl fault is cut by intragranular, transgranular and grain boundary microfractures. In detrital quartz grains, microfractures occur as open microfractures, microfractures sealed by calcite and laumontite, or as fluid-inclusion planes (FIP). All microfracture types increase in density towards the

ultracataclasite layer of the Punchbowl fault. The zone of microfracture damage associated with the Punchbowl fault extends approximately 100 m from the ultracataclasite layer (fault surface) as defined by the decrease in microfracture density to regional, background levels. Cross-cutting relations between microfractures and cements, and the density distribution of microfractures relative to the fault, indicate that the majority of microfractures are genetically related to faulting and that, in general, FIP formed early and open microfractures formed late. The preferred orientation of microfractures varies with distance from the ultracataclasite layer of the Punchbowl fault, and fabric domains approximately correlate with the fault core, damage zone, and undeformed host rock of the Punchbowl fault. The dominant preferred orientation of microfractures throughout the damage zone is perpendicular to the slip direction of the Punchbowl fault, which implies that the average orientation of the maximum principal compressive stress within the damage zone was nearly normal to the fault surface. The consistency in the preferred orientation of FIP, from early time periods, and open microfractures, from late time periods, suggests that the average stress orientation in the damage zone of the fault was similar throughout most of the fault history. Overall, the preferred orientation and timing of microfractures are most consistent with fabric development by stress cycling associated with slip on a geometrically irregular, relatively weak fault surface. However, the microfracture fabric in the innermost damage zone and fault core also may record wear associated with the passage of many earthquake ruptures. The preferred orientation of microfractures in the outermost portion of the damage zone may record an early stage of faulting under a paleostress field consistent with Andersonian faulting.

Acknowledgements

We thank David Wilson and Leslie Neal for assistance in the field, Ray Guillemette for his expertise on the microprobe and for preparing the elemental maps, Steve Dorobek and his students for their help and advice in obtaining cathodoluminescence images, and Dave Numer and Jack Farley for their continued assistance with our research in the Devil's Punchbowl Los Angeles County Park. Thorough reviews by Jafar Hadizadeh, Andreas Kronenberg, Steve Laubach, and Associate Editor, Tom Blenkinsop, are greatly appreciated. Financial support for this project was provided by U.S. Geological Survey Contract #1434-HQ-96-GR-02709.

References

Allmendinger, R.W., 1995. Stereonet v. 4.9.6 (shareware software, ftp site: http://silver.geo.cornell.edu). Dept. of Geological Sciences, Cornell University, Ithaca.

Anders, M.H., Wiltschko, D.V., 1994. Microfracturing, paleostress, and the growth of faults. Journal of Structural Geology 16, 795–815.

Anderson, E.M., 1942. The Dynamics of Faulting and Dyke Formation with Applications to Britain, Oliver and Boyd, Edinburgh.

Blenkinsop, T.G., 1990. Correlation of paleotectonic fracture and microfracture orientations in cores with seismic anisotropy at Cajon Pass drill hole, southern California. Journal of Geophysical Research 95, 11,143–11,150.

Blenkinsop, T.G., Sibson, R.H., 1992. Aseismic fracturing and cataclasis involving reaction softening within core material from the Cajon Pass drill hole. Journal of Geophysical Research 97, 5135–5144.

Borg, I., Friedman, M., Handin, J., Higgs, D.V., 1960. Experimental deformation of St. Peter sand: a study of cataclastic flow. In: Griggs, D., Handin, J. (Eds.), Rock Deformation. Geological Society America Memoir 79, pp. 133–192.

Brock, W.G., Engelder, T., 1977. Deformation associated with the movement of the Muddy Mountain overthrust in the Buffington Window, southeast Nevada. Bulletin of the Geological Association of America 88, 1667–1677.

Bruhn, R.L., Parry, W.T., Yonkee, W.A., Thompson, T., 1994. Fracturing and hydrothermal alteration in normal fault zones. Pure and Applied Geophysics 142, 609–644.

Chester, F.M., Chester, J.S., 1998. Ultracataclasite structure and friction processes of the San Andreas fault. Tectonophysics 295, 199–221.

Chester, F.M., Chester, J.S., 2000. Stress and deformation along wavy frictional faults. Journal of Geophysical Research 105, 23,421–23,430.

Chester, F.M., Logan, J.M., 1986. Implications for mechanical properties of brittle faults from observations of the Punchbowl Fault Zone, California. Pure and Applied Geophysics 124 (1/2), 79–106.

Chester, F.M., Logan, J.M., 1987. Composite planar fabric of gouge from the Punchbowl Fault, California. Journal of Structural Geology 9 (5/6), 621–634.

Chester, F.M., Evans, J.P., Biegel, R.L., 1993. Internal structure and weakening mechanisms of the San Andreas fault. Journal of Geophysical Research 98 (B1), 771–786.

Chester, F.M., Chester, J.S., Evans, J. P., Kirschner, D.L., Schulz, S.E., Evans, J.P., 2003. Structure of large-displacement, strike-slip fault zones in the brittle continental crust. In: Karner, G., Garry, D., Taylor, B., Driscoll, N., Kohlstedt, D.L. (Eds.). Rheology and Deformation of the Lithosphere at Continental Margins, Columbia University Press, New York, MARGINS Theoretical and Experimental Earth Science Series I.

Chester, J.S., Fletcher, R., 1997. Stress distribution and failure in anisotropic rock near a bend on a weak fault. Journal of Geophysical Research 102 (B1), 693–708.

Cowie, P.A., Scholz, C.H., 1992. Physical explanation for the displacement-length relationship of faults using a post-yield fracture mechanics model. Journal of Structural Geology 14 (10), 1133–1148.

Cox, B.F., Powell, R.E., Hinkle, M.E., Lipton, D.A., 1983. Mineral resource potential map of the Pleasant View Roadless Area, Los Angeles County, California. U.S. Geological Survey Miscellaneous Field Study Map, MF-1649-A, 1:62,500.

Dibblee, T.W. Jr, 1968. Displacements on the San Andreas fault system in the San Gabriel, San Benardino, and San Andreas Fault. Journal of Geophysical Research 98 (B1), 771–786.

Dibblee, T.W. Jr, 1987. Geology of the Devil's Punchbowl, Los Angeles County, California. In: Hill, M.L., (Ed.), Centennial Field Guide 1, Cordilleran Section, Geological Society of America, pp. 207–210.

Duyster, J., 2000. StereoNett Version 2.10 (shareware software, url site: http://homepage.ruhr-uni-bochum.de/Johannes.P.Duyster/stereo1.htm). Institut für Geologie, Bochum, Germany.

Engelder, J.T., 1974. Cataclasis and the generation of fault gouge. Geological Society of America Bulletin 85, 1515–1522.

Evans, J.P., Chester, F.M., 1995. Fluid-rock interaction in faults of the San Andreas system: inferences from San Gabriel fault rock geochemistry and microstructures. Journal of Geophysical Research 100 (B7), 13007–13020.

Flinn, D., 1977. Transcurrent fault and associated cataclasis in Shetland. Journal of the Geological Society of London 133, 231–248.

Friedman, M., 1963. Petrofabric analysis of experimentally deformed calcite-cemented sandstones. Journal of Geology 71, 12–37.

Friedman, M., 1969. Structural analysis of fractures in cores from the Saticoy Field, Ventura Co., California. American Association of Petroleum Geologists Bulletin 53, 367–389.

Kamb, W.B., 1959. Petrofabric observations from Blue Glacier, Washington, in relation to theory and experiment. Journal of Geophysical Research 64, 1908–1909.

Kowallis, B.J., Wang, H.F., Jang, B.A., 1987. Healed microcrack orientations in granite from Illinois borehole UPH-3 and their relationship to the rock's stress history. Tectonophysics 135, 297–306.

Kranz, R.L., 1983. Microcracks in rocks: a review. Tectonophysics 100, 449–480.

Laubach, S.E., 1989. Paleostress directions from the preferred orientation of closed microfractures (fluid-inclusion planes) in sandstone, East Texas basin, USA. Journal of Structural Geology 11, 603–611.

Laubach, S.E., 1997. A method to detect natural fracture strike in sandstones. American Association of Petroleum Geologist Bulletin 81, 604–623.

Lespinasse, M., Pecher, A., 1986. Microfracturing and regional stress field: a study of the preferred orientation of fluid-inclusion planes in a granite from the Massif Central, France. Journal of Structural Geology 8, 169–180.

Little, T.A., 1995. Brittle deformation adjacent to the Awatere strike-slip fault in New Zealand: faulting patterns, scaling relationships, and displacement partitioning. Geological Society of America Bulletin 107 (11), 1255–1271.

Martel, S.J., 1990. Formation of compound strike-slip fault zones, Mount Abbot quadrangle, California. Journal of Structural Geology 12, 869–882.

Milliken, K.L., Laubach, S.E., 2000. Brittle deformation in sandstone diagenesis as revealed by scanned cathodoluminescence imaging with application to characterization of fractured reservoirs. In: Pagel, M., Barbin, V., Blac, P., Ohnenstetter, D. (Eds.), Cathodoluminescence in Geosciences, Springer, New York, pp. 225–243.

Moore, D.E., Lockner, D.A., 1995. The role of microcracking in shear-fracture propagation in granite. Journal of Structural Geology 17, 95–114.

Noble, L.F., 1954. Geology of the Valyermo quadrangle and vicinity, California. U.S. Geological Survey Map GQ-50.

Power, W.L., Tullis, T.E., 1991. Euclidean and fractal models for the description of rock surface roughness. Journal of Geophysical Research 96, 415–424.

Saucier, F., Humphreys, E., Weldon, R., 1992. Stress near geometrically complex strike-slip faults: application to the San Andreas fault at Cajon Pass, southern California. Journal of Geophysical Research 97 (B4), 5081–5094.

Scholz, C.H., 1987. Wear and gouge formation in brittle faulting. Geology 15, 493–495.

Scholz, C.H., 1990. The Mechanics of Earthquakes and Faulting, Cambridge University Press, New York.

Scholz, C.H., Aviles, C.A., 1986. The fractal geometry of faults and faulting. American Geophysical Union Monograph 37, 147–155.

Scholz, C.H., Dawers, N.H., Yu, J.Z., Anders, M.H., Cowie, P.A., 1993. Fault growth and fault scaling laws: preliminary results. Journal of Geophysical Research 98, 21951–21961.

Schulz, S.E., Evans, J.P., 1998. Spatial variability in microscopic deformation and composition of the Punchbowl fault, southern California: implications for mechanisms, fluid-fault interaction and fault morphology. Tectonophysics 295, 223–244.

Shipton, Z.K., Cowie, P.A., 2001. Damage zone and slip-surface evolution over m to km scales in high-porosity Navajo sandstone, Utah. Journal of Structural Geology 23, 1825–1844.

Sibson, R.H., 1986. Brecciation processes in fault zones: inferences from earthquake rupturing. Pure and Applied Geophysics 124, 159–175.

Sibson, R.H., 1989. Earthquake faulting as a structural process. Journal of Structural Geology 11, 1–14.

Sibson, R.H., 1995. Selective fault reactivation during basin inversion; potential for fluid redistribution through fault-valve action. In: Buchanan, J.G., Buchanan, P.G. (Eds.), Basin Inversion. Geological Society Special Publications 88. Geological Society of London, London, UK, pp. 3–19.

Smith, D.L., Evans, B., 1984. Diffusional crack healing in quartz. Journal of Geophysical Research 89, 4125–4135.

Vermilye, J.M., Scholz, C.H., 1998. The process zone: a microstructural view. Journal of Geophysical Research 103, 12223–12237.

Wallace, R.E., Morris, H.T., 1986. Characteristics of faults and shear zones in deep mines. Pure and Applied Geophysics 124, 107–125.

Wang, C.-Y., Sun, Y., 1990. Oriented microfractures in Cajon Pass drill cores: stress field near the San Andreas fault. Journal of Geophysical Research 9, 11,135–11,142.

Weldon, R.J., II, Meisling, K.E., Alexander, J., 1993. A speculative history of the San Andreas fault in the central Transverse Ranges, California. In: Powell, R.E., Weldon II, R.J., Matti, J.C. (Eds.), The San Andreas Fault System: Displacement, Palinspastic Reconstruction, and Geologic Evolution. Geological Society America Memoir 178, pp. 161–198.

Wilson, J.E., 1999. Microfracture fabric of the Punchbowl fault zone, San Andreas system, California. M.S. thesis, Texas A&M University.

Wong, T.-F., David, C., Zhu, W., 1997. The transition from brittle faulting to cataclastic flow in porous sandstones: mechanical deformation. Journal of Geophysical Research 102 (B2), 3009–3025.

Woodburne, M.O., 1975. Cenozoic stratigraphy of the Transverse Ranges and adjacent areas, southern California. Geological Society of America Special Paper 162.

Zoback, M., Mount, V., Suppe, J., Eaton, J., Healy, J., Oppenheimer, D., Reasenberg, P., Jones, L., Raleigh, C., Wong, I., Scotti, O., Wentworth, C., 1987. New evidence on the state of stress of the San Andreas fault system. Science 238, 1105–1110.